cosmetics

MDPI

Article

Anti-Photoaging Effects of *Kaempferia galanga* Extract: From Cell-Based Studies to Microemulsion Development

Kunlathida Luangpraditkun, Jinnipha Pajoubpong, Piyachat Kasemkiatsakul, Ngamrayu Ngamdokmai, Mayuree Poonasri, Somnathtai Yammen and Boonyadist Vongsak *

Faculty of Pharmaceutical Sciences, Burapha University, Chonburi 20131, Thailand; kunlathida.lu@go.buu.ac.th (K.L.); jinnipha.pa@go.buu.ac.th (J.P.); piyachat.k.sakul@gmail.com (P.K.); ngamrayu.ng@go.buu.ac.th (N.N.); mmayuree.p@gmail.com (M.P.); somnathtai.ya@go.buu.ac.th (S.Y.)
* Correspondence: boonyadist@go.buu.ac.th

Abstract

Ozone layer depletion exacerbates UV-induced skin damage, including oxidative stress and DNA lesions, thereby increasing the risk of photoaging and malignant transformation. Natural extracts have gained increasing attention as a photoprotective ingredient in cosmeceutical products. *Kaempferia galanga*, a species in the Zingiberaceae family traditionally used for skin-related treatment and listed in the CosIng database, exhibits multiple biologically relevant properties; however, its anti-photoaging and anti-photo-senescence effects in human dermal fibroblasts remain unexplored. This study investigated the in vitro photoprotective effects of *K. galanga* extract against UVB-induced photoaging and cellular senescence in human dermal fibroblasts. The ethanolic extract of *K. galanga* rhizomes (EKGRs) contained ethyl *p*-methoxycinnamate (EPMC) as a major constituent (33.7 ± 3.7% (*w*/*w*) of the crude extract), identified by HPLC-UV. Additionally, EKGR exhibited significant protective effects in UVB-irradiated fibroblasts. EKGR showed no cytotoxicity at concentrations up to 50.0 μg/mL, as determined by the MTT assay. EKGR pretreatment significantly reduced UVB-induced cellular senescence in human dermal fibroblasts compared with UVB-exposed cells (22.2 ± 2.7% vs. 36.7 ± 8.0%). Furthermore, pretreatment with EKGR prior to UVB exposure resulted in a significant increase in pro-collagen type I production (37,075.1 ± 7532.2 pg/mL) and a concomitant decrease in MMP-1 secretion (25,754.1 ± 4042.0 pg/mL) relative to UVB-exposed cells (26,845.8 ± 1454.6 and 39,910.8 ± 6035.1 pg/mL, respectively). To demonstrate formulation feasibility, EKGR was incorporated into an oil-in-water microemulsion, which exhibited concentration-dependent SPF enhancement. Collectively, these findings demonstrate the photoprotective efficacy of EPMC-rich EKGR and highlight its potential as a cosmeceutical ingredient for mitigating UVB-induced photo-senescence and skin aging, with an additional SPF boosting effect. To our knowledge, this study provides the first evidence of EKGR-mediated protection against UVB-induced cellular senescence in human dermal fibroblasts.

Keywords: *Kaempferia galanga* L.; UVB; fibroblasts; anti-senescence; MMP-1; pro-collagen type I; microemulsion

Check for updates

Academic Editor: Aura Rusu

Received: 7 February 2026
Revised: 11 April 2026
Accepted: 15 April 2026
Published: 21 April 2026

Copyright: © 2026 by the authors. Licensee MDPI, Basel, Switzerland. This article is an open access article distributed under the terms and conditions of the Creative Commons Attribution (CC BY) license.

1. Introduction

Human skin is the outermost layer of the body, acting as the primary defensive barrier against environmental factors. Ultraviolet (UV) radiation has been studied for a long time and is one of the main stressors contributing to inflammation, aging and

skin cancer [1–6]. Specifically, UVB (280–320 nm), a highly energetic component of UV radiation, is primarily absorbed in the epidermis but can also penetrate into the upper papillary dermis [3,7,8]. A skin cell's DNA can absorb UVB photons directly. UVB also provokes free radicals indirectly. Consequently, prolonged exposure to UVB induces the overproduction of cellular reactive oxygen species (ROS), causing oxidative stress, DNA fragmentation and damage to other macromolecules [9,10]. These alterations are associated with increased inflammation, collagen degradation, and the accumulation of senescent fibroblasts in the dermis. Ultimately, these signs of aging, including fine lines, sagging, and wrinkles, appear prematurely [11]. It is well-documented that excessive ROS is a dominant event that triggers the upregulation of matrix metalloproteinases (MMPs), which degrade components of the dermal extracellular matrix (ECM). MMP-1 especially plays a crucial role in the degradation of type-1 collagen, the major structural protein comprising approximately 80–90% of the skin. Upon exposure to UVB, the activated MMP-1 is induced by ROS via cytoplasmic mitogen-activated protein kinase (MAPK) signaling/activator protein-1 (AP-1) pathways, bringing about collagen breakdown, loss of ECM integrity and altering skin structure [12]. In addition, nuclear factor kappa B (NF-κB), an activator of the inflammatory response, is activated, leading to autocrine cytokine release. This signaling provokes overexpression of pro-inflammatory cytokines such as tumor necrosis factor-α (TNF-α) and interleukin-6 (IL-6) [6,13]. Beyond stimulating the overproduction of ECM-modifying enzymes and inflammatory cytokines, UVB exposure has also been associated with senescence-associated beta-galactosidase (SA-β-Gal) upregulation, which is recognized as a hallmark enzyme of cellular senescence [14]. A senescent fibroblast is a type of skin cell that has permanently stopped dividing due to aging or even stress; however, it remains metabolically active [15,16]. Exciting research has found that using plant extracts may help rejuvenate aged fibroblasts by reversing aspects of their aging phenotype [13].

Kaempferia galanga L. ("Proh hom" in Thai) is a plant belonging to the family of Zingiberaceae, distributed in Southeast Asia including Thailand. *K. galanga* is considered a valuable medicinal plant rich in bioactive compounds, particularly those derived from its rhizomes. Several studies have revealed that rhizome extracts contain important essential oils such as cinnamic acid derivatives. The biological efficacy of *K. galanga* essential oil is largely influenced by its high content of ethyl *p*-methoxycinnamate (EPMC) and ethyl cinnamate [17]. The biological activities of ethanolic extracts of *K. galanga* rhizome (EKGR), such as antioxidation [18,19], anti-collagenase [19], anti-elastase [19], anti-inflammatory [17,20], antibacterial [21,22], and wound-healing activities [23,24] and UV absorption properties [17,25,26], have been reported. To date, few studies have addressed the protective effects of EKGR against UVB-induced cellular aging, specifically focusing on the suppression of UVB-induced fibroblast senescence. A prior study has reported that *K. galanga* Linn. rhizome extracts exhibited anti-aging activity, including anti-collagenase and anti-elastase activity, based on an in vitro chemical-based study. Investigations regarding the photoaging ability of *K. galanga* extract in in vitro cell-based assays are lacking. Hence, this study was designed with the rational study objective of elucidating the photoprotective effects of EKGR against UVB-induced fibroblast aging by examining the expression profiles of key proteins and enzymes involved in the oxidative stress response and extracellular matrix regulation. Specifically, this study focused on the modulation of biomarkers associated with matrix degradation and cellular senescence. Furthermore, for further application of the extract to increase its value, its potential applicability in cosmeceutical formulations was evaluated. Several studies have reported that flavonoids are a major class of polyphenolic compounds with significant biological and photoprotective properties. EPMC, a cinnamate derivative and the main constituent in EKGR, functions as an organic UVB filter due to its specific molecular structure [27]. EPMC absorbs high-energy photons and prevents

the transmission of harmful radiation to the skin. Thus, EKGR was incorporated into the oil phase of an oil-in-water microemulsion system, followed by assessments of its sun protection factor (SPF) performance and formulation stability.

Microemulsions are single-phase systems composed of water, oil, and one or more amphiphiles, forming a thermodynamically stable isotropic solution. They appear optically transparent or translucent because the droplet size of the dispersed phase is smaller than the wavelength of visible light, typically in the range of 10–100 nm. Depending on composition, microemulsions can be categorized as oil-in-water (O/W), water-in-oil (W/O) or bicontinuous systems [28–30]. In cosmetic applications, microemulsions are widely utilized to enhance the stability and solubility of active compounds, particularly those that are poorly soluble or unstable in aqueous environments [31–33]. In this study, ethyl oleate was selected as the oil phase because it is an ester-based oil capable of solubilizing both hydrophilic and lipophilic compounds. Tween 80 was chosen as the primary surfactant due to its high hydrophilic–lipophilic balance (HLB) value and critical packing parameter (CPP) below 0.33, favoring the formation of O/W microemulsions—our desired system type. A co-surfactant, 1,2-hexanediol, was included to further enhance interfacial fluidity at the oil–water interface. Additionally, 1,2-hexanediol provides humectant benefits, making it suitable for cosmetic formulations.

2. Materials and Methods

2.1. The Preparation of K. galanga Rhizome Extract

The rhizomes of *K. galanga* (Aromatic Ginger) were purchased from a herbal garden in Surin province. A small number of rhizomes were planted and identified by an expert to confirm the species. The fresh rhizomes were cleaned to wash all the dirt off and cut into thin slices. These thin pieces were dried at 45 °C for 48 h or until dryness using a hot air oven (KH-100A, Kenton, Guangzhou, China). These dried rhizomes were pulverized into a fine powder. A simple maceration method was selected to prepare *Kaempferia galanga* L. rhizome extract. 95% ethanol (AR grade, Fisher Scientific, Loughborough, UK) was chosen for solvent extraction with a ratio of 1:10 *w*/*v* (dried powder to ethanol). The maceration process was performed for 48 h with light protection. The ethanolic extract of *K. galanga* rhizome (EKGR) was filtered using filter paper (Whatman No. 1, 90 mm diameter, Cytiva, Amersham, UK) to remove any residuals. The organic solvent was then evaporated using a rotary evaporator (RV8 V, IKA, Staufen, Germany). The percent yield (% yield) of EKGR was calculated and EKGR was stored at 20 °C with light protection for further studies.

2.2. Quantification of Ethyl-p-Methoxy Cinnamate in EKGR

The amount of ethyl *p*-methoxycinnamate (EPMC) in EKGR was measured using high-performance liquid chromatography with ultraviolet detection (HPLC-UV). The stationary phase was a C18 column (ACE® C18 (150 mm × 4.6 × mm, 5 µm; Advanced Chromatography Technologies, Aberdeen, UK). The mobile phase consisted of 40% water and 60% acetonitrile. Each sample was run in isocratic mode for 30 min [34]. A photodiode array was used as a detector. A standard EPMC with ≥98.0% purity was purchased from Toronto Research Chemicals Inc. (TRC-M262155, Lot 6-NOT-120-3, Toronto, ON, Canada). The column temperature, the injection volume and flow rate were set at 30 °C, 10 µL and 1.0 mL/min, respectively. Absorbance was measured at a wavelength of 308 nm. The EPMC content in EKGR was calculated using a standard calibration curve. All experiments were performed in triplicate.

2.3. Cell Culture

Primary adult human dermal fibroblasts (HDFs, PCS-201-012) were purchased from ATCC (Lot No.81201212, Manassas, VA, USA). A certificate of approval to conduct biosafety research with IBC 039/2567 was approved by Burapha University ethics committee. The cells were counted (5000 cells/cm^2) and cultured in high-glucose Dulbecco's Modified Eagle Medium (DMEM) supplemented with 100 units/mL of penicillin, 100 units/mL of streptomycin, 1 mg/mL amphotericin B, and 10% fetal bovine serum (FBS) in humidified air containing 5% CO_2 atmosphere at 37 °C. The medium was changed every 2–3 days. The subculture was performed at 70–80% of cell confluence.

2.4. Evaluation of Cell Viability

The effect of EKGR on cell viability was assessed by MTT assay. HDFs at passage 5–8 (1.0×10^4 cells/well) were plated into a 96-well plate and treated with or without EKGR at concentrations of 3.1–50.0 μg/mL for 24 h. Then, the culture media in each well were replaced with fresh serum-free DMEM containing MTT (500 μg/mL) and incubated for 4 h at 37 °C in humidified air containing 5% CO_2. After incubation, the culture medium was removed and formazan crystals were solubilized by DMSO. The absorbance was determined at 490 nm using a microplate reader (FLUOstar® Omega, BMG LABTECH, Software version: 6.20, Ortenberg, Germany).

2.5. Evaluation of UVB-Induced Fibroblast Senescence Using the Senescence-Associated β-Galactosidase (SA-β-Gal) Assay

HDFs at passage 8–15 (1.0×10^4 cells/well) were grown in a 96-well plate at 37 °C in humidified air containing 5% CO_2 for 24 h. After washing the cells twice with sterile PBS, a thin layer of PBS was added to cover HDFs. Then HDFs were exposed to UVB irradiation (UVB T5 HO lamp, Reptisun®, Germany) at various doses (0, 17.5, 35 and 70 mJ/cm^2) to determine the threshold that significantly induces cellular senescence compared to non-UVB-exposed cells. The intensity of UVB was measured using a digital UVB radiometer (Solarmeter, Solartech Inc., PA, USA). The average irradiance was 0.1167 mW/cm^2. Thus, the HDFs were exposed to UVB for 0, 150, 300, and 600 s, respectively. After UVB exposure, HDFs were further incubated in supplement-free medium for 24 h. The cells were washed twice with PBS and fixed with fixing solution for 5 min at room temperature. After washing with PBS thrice, cells were incubated with SA-β-Gal staining solution (ab65351, Abcam, Cambridge, UK) overnight at 37 °C then thrice washed with PBS. After washing, the stained cells were examined under a brightfield microscope. The percentage of SA-β-Gal-positive cells was estimated, and triplicate experiments were performed.

2.6. Evaluation of Photoprotective Effects of EKGR on UVB-Induced Fibroblast Aging

2.6.1. SA-β-Gal Expression

HDFs at passage 8–15 (1.0×10^4 cells/well) were grown in a 96-well plate at 37 °C in humidified air containing 5% CO_2 for 24 h. Cells were washed twice before incubating with serum-free DMEM containing EKGR (50 μg/mL) for 24 h. Cells were washed twice with PBS and exposed to a UVB dose of 35 mJ/cm^2, followed by further incubation in serum-free DMEM for 24 h. After that, each cell group was analyzed for SA-β-Gal expression as mentioned above. Finally, the percentage of SA-β-Gal-positive cells was assessed. Triplicate experiments were performed.

2.6.2. Pro-Collagen Type 1 and MMP-1 Expression

HDFs at passage 8–15 (3.0×10^5 cells/well) were grown in a 6-well plate at 37 °C in humidified air containing 5% CO_2 for 24 h. Cells were washed twice before incubating with serum-free DMEM containing EKGR (50 μg/mL) for 24 h. Cells were washed twice with

PBS and exposed to a UVB dose of 35 mJ/cm^2, followed by further incubation in serum-free DMEM for 24 h. Then the culture medium was collected to analyze the levels of pro-collagen type I and MMP-1 using a pro-collagen type 1 ELISA kit (ab210966, Abcam, Cambridge, UK) and MMP-1 ELISA kit (ab215082, Abcam, Cambridge, UK), respectively, according to the manufacturer's instructions. Finally, the absorbance was measured at 450 nm using a microplate reader (FLUOstar® Omega, BMG LABTECH, Ortenberg, Germany). The pro-collagen type 1 and MMP-1 contents in the supernatant were calculated using a standard calibration curve. All experiments were performed in triplicate.

2.7. Pseudo-Ternary Phase Diagram Construction

Pseudo-ternary phase diagrams were constructed using ethyl oleate (EO) as the oil phase and a mixed surfactant system comprising Tween 80 (T80) and 1,2-hexanediol (HD). The surfactant mixture (Smix) was prepared at fixed weight ratios of T80:HD (4:1 and 3:1). EO and Smix were then combined at EO-to-Smix weight ratios of 1:9, 2:8, 3:7, 4:6, 5:5, and higher as appropriate, with a total mixture of weight 2 g.

Distilled water was incrementally added to each mixture in 0.5 g steps under gentle stirring at ambient temperature. For example, at an EO-to-Smix ratio of 1:9, 0.5 g of water was initially added to 2 g of the EO–Smix mixture in a test tube, while in a separate tube, 1.0 g of water was added to 2 g of the EO–Smix mixture to obtain different compositions. Samples were then allowed to equilibrate for 24 h.

Phase behavior was visually evaluated based on clarity (clear or turbid) and phase separation (single or multiple phases). To more precisely determine phase boundaries, additional samples were prepared using smaller water increments (as low as 0.1 g) near the transition regions.

Compositions at which phase separation or turbidity was observed were expressed as weight percentages of EO, Smix, and water, and used to delineate the boundary of the single-phase region in the pseudo-ternary phase diagram. Cosmetic-grade EO, T80, and HD were used in all experiments.

2.8. Particle Size Analysis of Microemulsions

EO, mixed surfactants of T80 and HD, and water were blended at weight ratios of 10:65:25, 20:65:15, and 30:65:5 using a simple emulsification method. After 24 h of equilibration, the samples were transferred into cuvettes, and particle size was measured using dynamic light scattering (DLS) without further dilution at 25 °C. The refractive index of the material was set at 1.47.

2.9. Viscosity Measurement of Microemulsions

EKGR, EO, mixed surfactants of T80 and HD, and water were blended at weight ratios of 0.5:9.5:65:25, 0.5:19.5:65:15, and 0.5:29.5:65:5 using a simple emulsification method. After 24 h of equilibration, the viscosity profiles were measured at 25 ± 0.5 °C using a Kinexus Lab+ rheometer (KNX2112, Malvern Instruments Limited, Worcestershire, UK) equipped with a cone-and-plate geometry.

2.10. Sun Protection Factor (SPF) Determination

Microemulsion formulations containing EKGR, EO, mixed surfactants of T80 and HD, and water were prepared at weight ratios of 0.5:29.5:65:5, 0.75:29.25:65:5, and 1:29:65:5 using a simple mixing method under gentle stirring at ambient temperature. After 24 h of equilibration, 1.0 g of each ME sample was weighed and diluted with 95% ethanol to obtain a final concentration of 0.02% *w*/*v*. The resulting solution was transferred into a 1 cm quartz cuvette. UV absorption profiles were recorded over the range of 240–400 nm at 1 nm intervals using a Hitachi U-2900 spectrophotometer (Hitachi High-Technologies

Corporation, Tokyo, Japan), without further filtration. Each formulation was tested in quintuplicate (n = 5), and SPF values were expressed as mean ± standard deviation (SD). One-way ANOVA followed by Tukey's post hoc test was performed to evaluate differences between extract concentrations (1.00%, 0.75%, and 0.50%).

The SPF values were calculated using the following equation according to a published method [35]:

$$SPF_{spectrophotometric} = CF \times \sum_{\lambda=290}^{320} EE(\lambda) \times I(\lambda) \times Abs(\lambda)$$

where $EE(\lambda)$ is the erythemal effect spectrum, $I(\lambda)$ is the solar intensity spectrum, and the product $EE(\lambda) \times I(\lambda)$ is constant, as determined by Sayre et al. [36]. The correction factor (CF) was set to 10.

For data analysis, absorbance values at 290, 295, 300, 305, 310, 315, and 320 nm were multiplied by the corresponding $EE(\lambda) \times I(\lambda)$ values (see Supplementary Materials). The summation of these values was then multiplied by the correction factor (CF = 10).

2.11. Stability Testing: Chemical (Assay), Physical (Particle Size), Appearance Evaluation

ME A–C formulations, with and without 0.5% w/w EKGR, were stored in clear glass jars with aluminum caps for 1 month under four conditions: −20 °C, 4 ± 2 °C, 25 ± 2 °C, and 40 ± 2 °C/75% RH. For chemical stability, the EPMC content was quantified by HPLC as previously described. Test sample solutions were prepared by diluting 10 mg of each ME containing 0.5% w/w EKGR with 500 µL methanol. For physical stability, the particle sizes of ME A–C without EKGR were measured by DLS following a previously described method. In addition, appearance (e.g., phase separation, clarity, and precipitation) was visually evaluated both upon reaching equilibrium (after 24 h) and after 1 month.

2.12. Statistical Analysis

Data are presented as means ± standard deviation (SD). Cell studies were performed in triplicate (n = 3), SPF measurements were conducted in quintuplicate (n = 5), and the content of EPMC was determined in triplicate (n = 3). Descriptive statistics were applied to all measurements. Inferential statistical analysis was performed where appropriate using one-way ANOVA followed by Tukey's post hoc test to evaluate differences between groups, with the significance level set at $p < 0.05$.

3. Results

3.1. Characteristics of an Ethanolic Extract of K. galanga Rhizome (EKGR) and Its Ethyl-p-Methoxy Cinnamate (EPMC) Content

EKGR is characterized as a dark brown viscous liquid, as shown in Figure 1. The percent yield of EKGR was 8.25 ± 0.41.

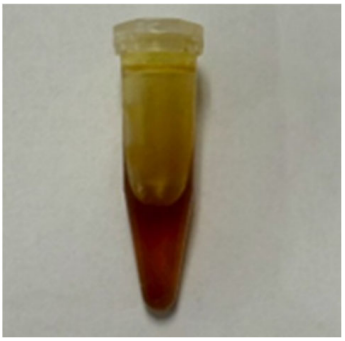


Figure 1. The characteristics of an ethanolic extract of *K. galanga* rhizome.

The content of EPMC, the major bioactive compound in EKGR, was quantified using HPLC-UV. The chromatograms of the EPMC standard (≥98.0%) and EKGR are shown in Figure 2. The content of EPMC in EKGR was calculated using an EPMC standard calibration curve. The EPMC content in EKGR was determined to be 33.7 ± 3.7% (*w*/*w*).

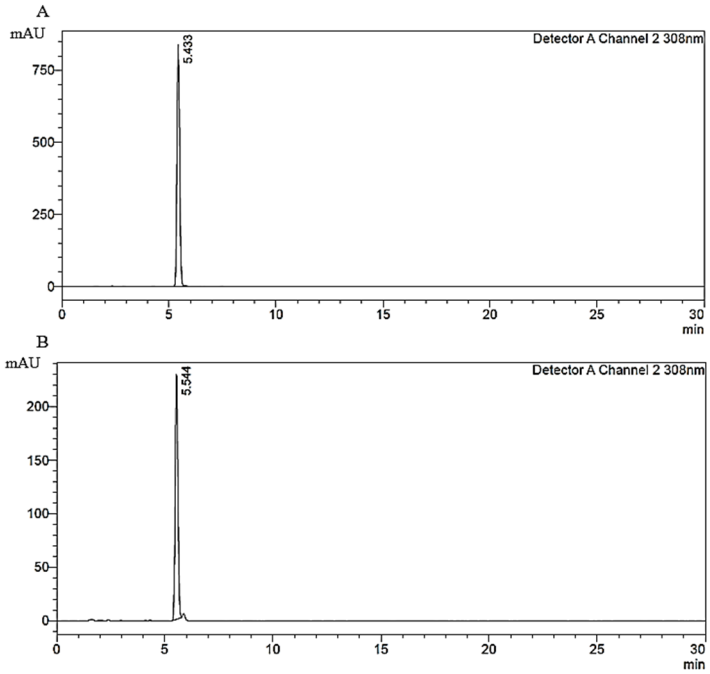


Figure 2. HPLC chromatogram of (**A**) EPMC standard (≥98.0%) and (**B**) an ethanolic extract of *K. galanga* rhizome (EKGR). Absorbance was measured at 308 nm.

3.2. The Effect of EKGR on Cell Viability in Primary Adult Human Dermal Fibroblasts (HDFs)

Due to the solubility limitation of the extract, the concentration used in this study could not exceed 50.0 µg/mL. Thus, to estimate the cytotoxicity of EKGR, HDFs were treated with EKGR at concentrations ranging from 3.1 to 50.0 µg/mL for 24 h. The cell viability was evaluated based on the MTT assay. The percentages of cell viability and cell morphology of each group are shown in Figure 3 and Figure 4, respectively.

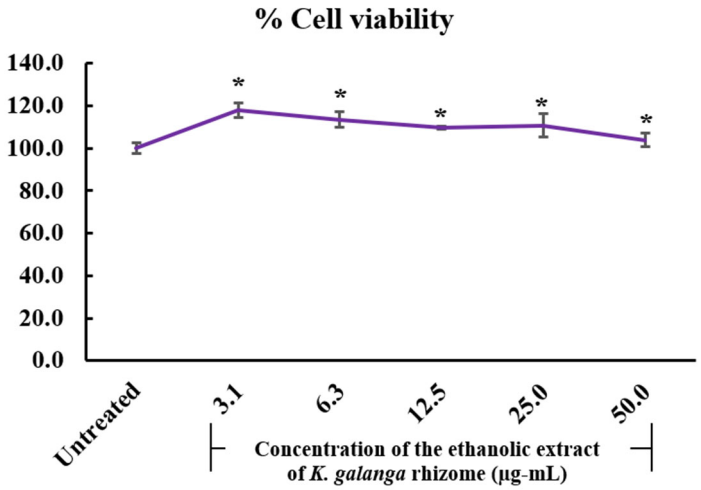


Figure 3. Viability of primary adult human dermal fibroblasts (HDFs) with and without an ethanolic extract of *K. galanga* rhizome (EKGR) treatment for 24 h. Results are expressed as % cell viability relative to untreated cell group (where the OD of untreated was set to 100%). Each bar represents the mean ± S.D. of three independent experiments. * $p < 0.05$, compared with the untreated cell group, as determined by one-way ANOVA followed by Tukey's HSD post hoc test.

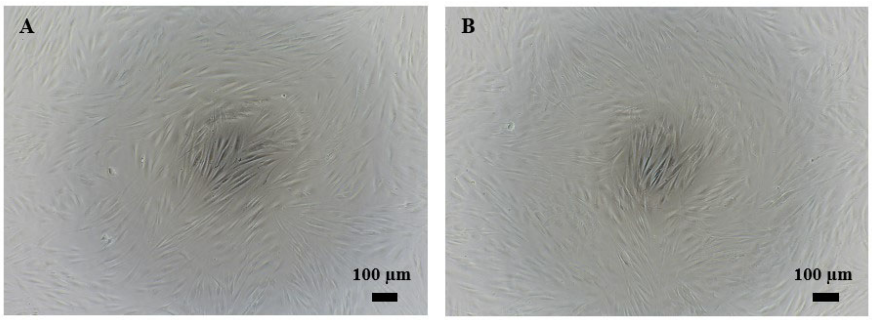


Figure 4. The cell morphology of (**A**) primary adult human dermal fibroblasts (HDFs) without treatment (untreated cells) and (**B**) HDFs treated with an ethanolic extract of *K. galanga* rhizome (EKGR, 50.0 µg/mL) for 24 h. Representative microscopic images at 100×.

The results showed that EKGR at concentrations of 3.1, 6.3, 12.5, 25.0, and 50.0 µg/mL significantly increased the percentage of cell viability (117.9 ± 3.5, 113.5 ± 3.7, 109.6 ± 0.6, 110.7 ± 5.3, and 103.8 ± 3.3 respectively) compared to untreated cells (100.0 ± 2.4). In particular, the highest concentration of EKGR (50.0 µg/mL) did not show any toxicity and did not affect the normal cell morphology; this was selected to study the photoprotective effects of EKGR in further experiments.

3.3. The Effect of UVB-Induced HDF Senescence

In this study, UVB-induced senescence resulted in different effects following various doses (17.5, 35.0 and 70 mJ/cm^2). The percentage of SA-β-Gal-positive cells in each group is exhibited in Figure 5 and the morphology, as well as SA-β-Gal-stained cells, is shown in Figure 6.

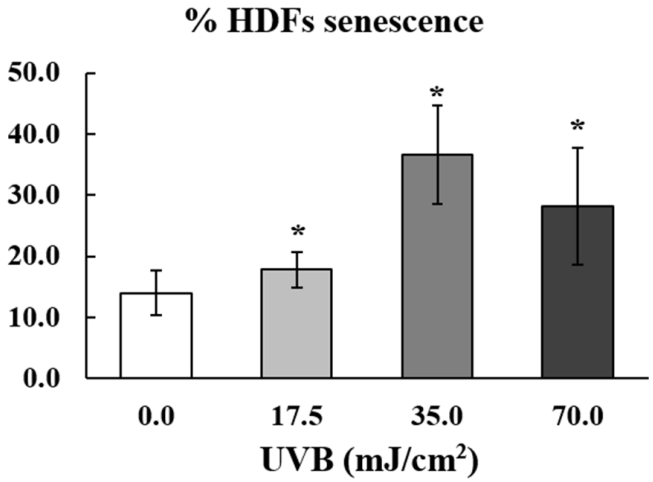


Figure 5. Percentages of SA-β-Gal-positive cells in non-UVB-exposed cells (control group) and in primary adult human dermal fibroblasts (HDFs) exposed to UVB doses of 17.5, 35.0 and 70.0 mJ/cm^2. Each bar represents the mean ± S.D. of three independent experiments. * $p < 0.05$, compared with the non-UVB-exposed cell group, as determined by one-way ANOVA followed by Tukey's HSD post hoc test.

The percentages of SA-β-Gal-stained cells of non-UVB- and UVB-exposed cells at doses of 17.5, 35.0, and 70.0 mJ/cm^2 were 14.0 ± 3.7, 17.8 ± 2.9, 36.7 ± 8.0, and 28.2 ± 9.5, respectively. The effect of these UVB doses affected the increase in the percent of SA-β-Gal-stained cells significantly. Although the lowest UVB dose had a significant effect on cell senescence, a higher dose (35.0 mJ/cm^2) was selected for subsequent studies because it not only affected the increase in the number of cells with SA-β-Gal activity but also influenced the morphology, leading to a clearly larger cell size compared to the non-UVB-exposed cell

group and those that received a low level of UVB. However, when the total dose of UVB was increased to 70 mJ/cm^2, it affected both senescence and cell death. Therefore, a UVB dose of 35.0 mJ/cm^2 was chosen for further studies to focus on cell senescence.

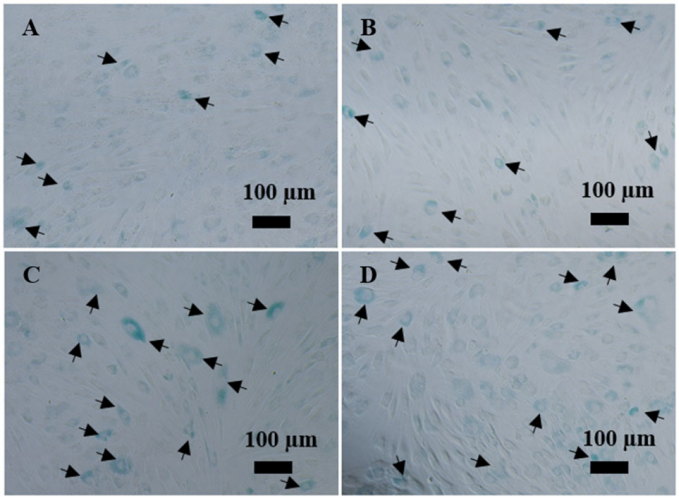


Figure 6. Representative phase-contrast microscopy images (200×) of (**A**) non-UVB-exposed cells (control) and primary adult human dermal fibroblasts (HDFs) exposed to UVB at different doses of (**B**) 17.5, (**C**) 35.0, and (**D**) 70.0 mJ/cm^2, used to analyze the quantity of senescent cells. The black arrows indicate cell staining SA-β-Gal activity.

3.4. Photoprotective Activities of EKGR upon UVB-Induced HDF Senescence

3.4.1. Senescence-Associated β-Galactosidase (SA-β-Gal)

This experiment was divided into three groups: non-UVB-exposed cells, cells exposed to a UVB dose of 35.0 mJ/cm^2 and cells pretreated with EKGR prior to exposing them to UVB. The percentage of SA-β-Gal-positive cells in each group is exhibited in Figure 7 and the morphology, as well as SA-β-Gal-stained cells, is shown in Figure 8.

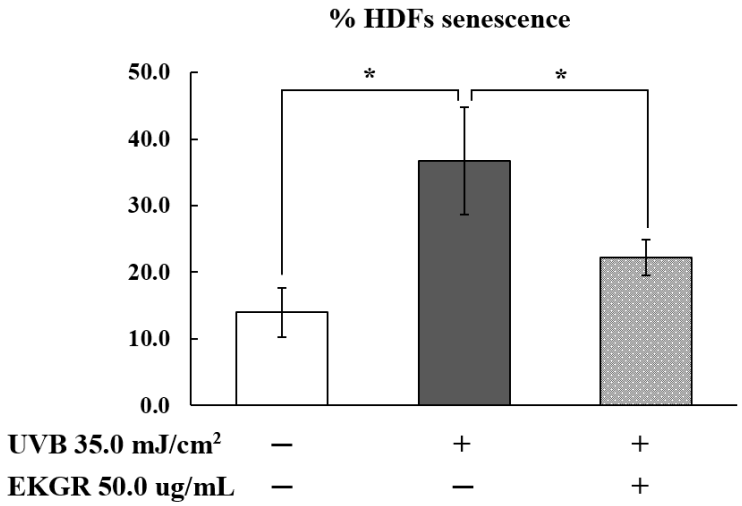


Figure 7. Percentages of SA-β-Gal-positive cells in non-UVB-exposed cells (control group), primary adult human dermal fibroblasts (HDFs) exposed to a UVB dose of 35.0 mJ/cm^2 (UVB group) and HDFs pretreated with an ethanolic extract of *K. galanga* rhizome (EKGR) for 24 h then exposed to UVB (UVB + EKGR group). Each bar represents the mean ± S.D. of three independent experiments. * $p < 0.05$; statistical comparisons among groups were performed using one-way ANOVA with Tukey's HSD post hoc test.

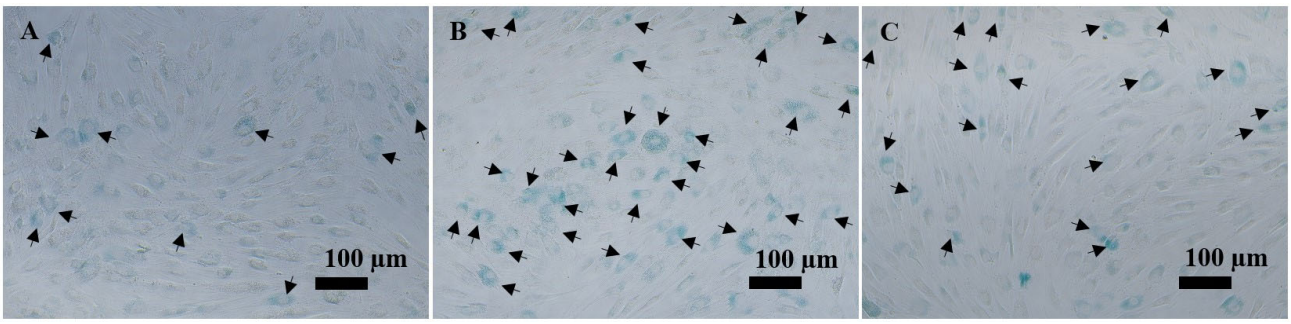


Figure 8. Representative phase-contrast microscopy images (200×) of (**A**) non-UVB-exposed cells (control), (**B**) primary adult human dermal fibroblasts (HDFs) exposed to a UVB dose of 35.0 mJ/cm^2 and (**C**) HDFs treated with an ethanolic extract of *K. galanga* rhizome (EKGR, 50.0 µg/mL) for 24 h then induced by UVB, used to analyze the quantity of senescent cells. The black arrows indicate cell staining SA-β-Gal activity.

As shown in Figure 7, the percentage of SA-β-Gal-stained HDFs in the control group (without EKGR pretreatment and UVB exposure) was 14.0 ± 3.7%, whereas in HDFs exposed to UVB (35 mJ/cm^2), the percentage of SA-β-Gal-positive cells was 36.7 ± 8.0%, indicating that the effects of UVB significantly increased fibroblast senescence by around 22.7%. Interestingly, pretreatment with EKGR prior to UVB exposure significantly decreased the SA-β-Gal-positive cells (22.2 ± 2.7%), suggesting that EKGR effectively protected the accumulation of senescent cells induced by UVB (it could reduce it by around 14.5%).

3.4.2. Pro-Collagen Type 1 and Matrix Metalloproteinase (MMP-1) Expression

The quantity of pro-collagen type 1 and MMP-1 in the culture medium was examined by ELISA.

The levels of pro-collagen type 1 and MMP-1 are shown in Figure 9. Obviously, UVB exposure reduced pro-collagen type 1 expression (26,845.8 ± 1454.6 pg/mL) compared with non-UVB-exposed cells (46,179.3 ± 2005.1 pg/mL), while cells pretreated with EKGR prior to UVB exposure significantly enhanced the expression level of pro-collagen type 1 (37,075.1 ± 7532.2 pg/mL). The important reason why UV radiation causes a collagen decrease is that it stimulates intracellular signaling pathways, altering the control of collagen-degrading enzymes like MMP-1 in an increased direction. This event degrades collagen in the matrix. This study confirmed that UVB resulted in an upregulation of MMP-1 secretion. The reported levels of MMP-1 in the non-UVB- and UVB-exposed cell groups were 14,473.6 ± 2358.8 and 39,910.8 ± 6035.1 pg/mL, respectively. Cells pretreated with EKGR prior to UVB exposure exhibited a significant decrease in MMP-1 levels (25,754.1 ± 4042.0 pg/mL). This suggests that EKGR may contribute to the preservation of pro-collagen type I through the inhibition of MMP-1 in UVB-induced HDFs.

3.5. Pseudo-Ternary Phase Diagram of the System

The pseudo-ternary phase diagrams of EO, mixed surfactants (T80 and HD at ratios of 4:1 or 3:1), and water are shown in Figure 10. Single-phase regions in both diagrams are shaded in blue. Although both diagrams display comparable single-phase areas, the diagram with a T80-to-HD ratio of 4:1 showed a slightly larger single-phase region and was therefore selected for developing the extract-loaded formulations (points A–C).

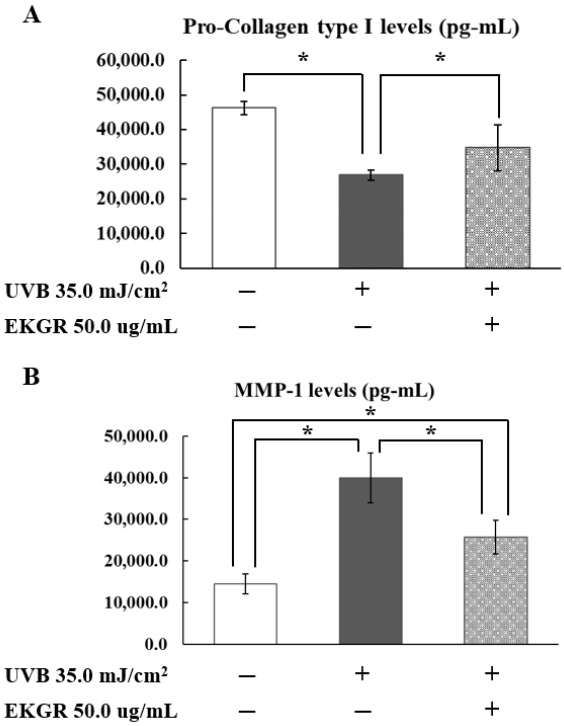


Figure 9. (**A**) Pro-collagen type I and (**B**) MMP-1 levels (pg/mL) in the supernatant, determined using an ELISA assay. The control group, primary adult human dermal fibroblasts (HDFs) exposed to UVB at dose of 35.0 mJ/cm^2 (UVB group) and HDFs pretreated with an ethanolic extract of *K. galanga* rhizome (EKGR) for 24 h then induced by UVB (UVB + EKGR group). Supernatant was collected at 24 h after UVB exposure. Each bar represents the mean ± S.D. of three independent experiments. * $p < 0.05$; statistical comparisons among groups were performed using one-way ANOVA with Tukey's HSD post hoc test.

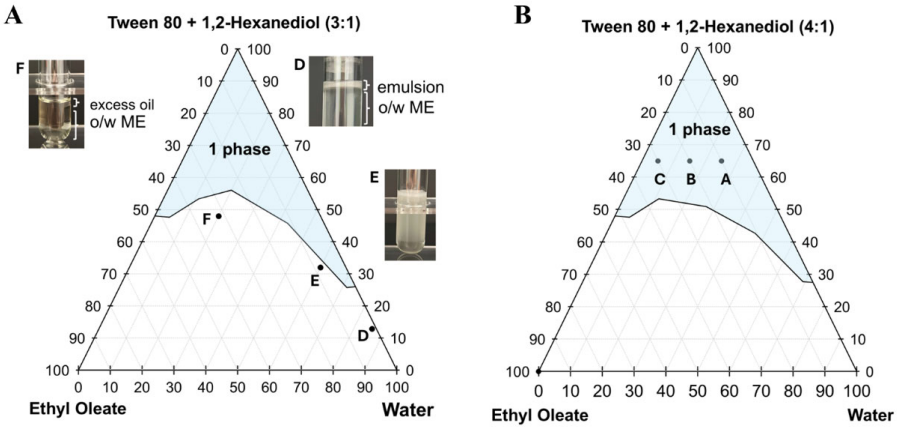


Figure 10. Pseudo-ternary phase diagrams composed of ethyl oleate, mixed surfactant (Tween 80 and 1,2-hexanediol), and water. Single-phase regions are shaded in blue. (**A**) Diagram for a Tween 80-to-1,2-hexanediol weight ratio of 3:1. Points D–F represent examples of two-phase systems obtained when water was titrated beyond the single-phase boundary. (**B**) Diagram for a Tween 80-to-1,2-hexanediol weight ratio of 4:1. Compositions corresponding to points A–C were selected for further characterization of droplet size and rheological behavior.

3.6. Particle Size Distribution of Microemulsions

The particle sizes of ME formulations A–C, corresponding to the compositions indicated as points A–C in Figure 10B, increased with increasing oil content (Table 1). The smallest droplets were observed in ME A (10% oil phase), with a mean diameter of approximately 4.9 nm. The droplet size increased to 7.5 nm for ME B (20% oil phase) and further to

17.2 nm for ME C (30% oil phase). A secondary large-size population was detected in both ME A and ME B, whereas ME C showed no evidence of such a population. These findings suggest that at lower oil contents, a small number of larger aggregates or transient clusters coexist with the predominant nano-sized droplets.

Table 1. Intensity-weighted particle size of microemulsion formulations.

Formulation	Weight Ratio (EO: T80 + HD: W)	Small Droplet Diameter (nm) ± SD	Large Domain Diameter (nm) ± SD *
ME A	10:65:25	4.89 ± 0.06	260.5 ± 19.4
ME B	20:65:15	7.48 ± 0.39	245.6 ± 21.7
ME C	30:65:5	17.20 ± 2.63	-

* Large domains attributed to the aggregation of oil droplets.

It is important to note that the particle size measurements were performed on extract-free microemulsions. EKGR strongly absorbs UVB, which would interfere with the DLS laser, potentially producing artificially reduced size readings. Therefore, droplet sizes obtained from extract-free microemulsions were reported in place of extract-loaded systems; however, the presence of the extract may alter droplet size.

3.7. Viscosity Profiles of Microemulsions

Viscosity profiles of ME A–C as a function of shear rate are shown in Figure 11. All extracted-loaded formulations exhibited constant viscosity across the tested shear-rate range (0.1–100 s^{-1}), indicating Newtonian flow behavior. This rheological behavior is characteristic of micellar solutions and Winsor I or II microemulsions [37]; this system is consistent with oil-in-water (O/W) microemulsions, as further supported by conductivity measurements. The Newtonian response indicates that MEs A–C possess isotropic internal structures.

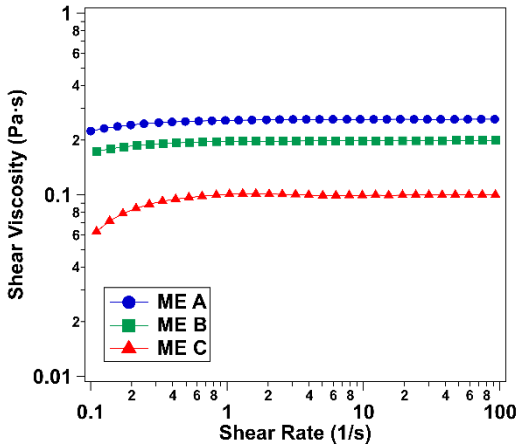


Figure 11. Viscosity profiles of *Kaempferia galanga* L. rhizome extract (EKGR)-loaded microemulsions. The compositions of the microemulsions (EKGR: EO: T80 + HD: W) were 0.5:9.5:65:25, 0.5:19.5:65:15, and 0.5:29.5:65:5 for ME A, ME B, and ME C, respectively. The T80-to-HD weight ratio was fixed at 4:1.

It is important to note that a single-phase, transparent appearance does not unequivocally confirm a microemulsion, as anisotropic structures such as hexagonal, cubic, or lamellar phases may also be present [38]. The observed Newtonian behavior, however, supports that MEs A–C are O/W microemulsions, consistent with the high HLB value of the surfactant (T80).

3.8. SPF of the Ethanolic Extract of K. galanga Rhizome (EKGR)-Loaded Microemulsions

The SPF of EKGR-loaded MEs increased with EKGR concentration in the range of 0.5–1% *w*/*w*, as shown in Figure 12 (see calculation details in the Supplementary Materials). SPF values were 6.8 ± 0.6, 10.8 ± 0.7, and 13.1 ± 0.9 for formulations containing 0.5%, 0.75%, and 1% EKGR, respectively. These results indicate that EKGR, which contains the major active compound ethyl *p*-methoxycinnamate (EPMC), possesses UVB absorption properties and can effectively enhance SPF values in microemulsion formulations.

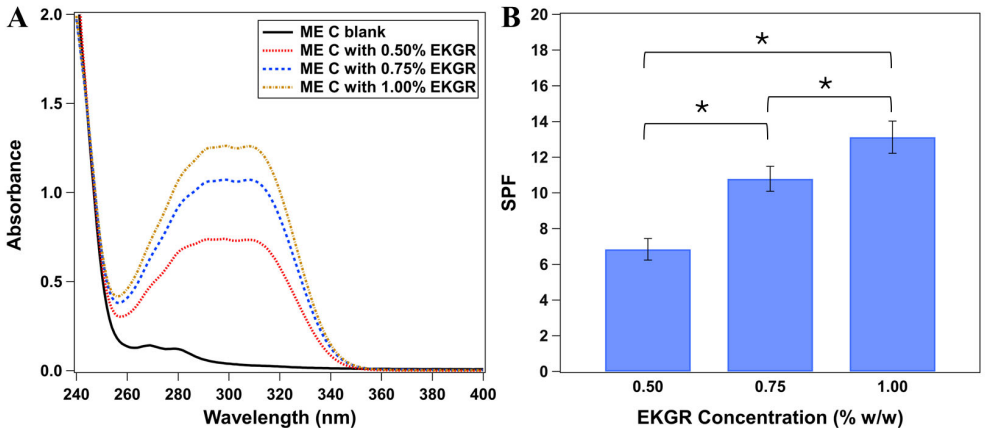


Figure 12. (**A**) UV absorbance profiles of ME C containing the ethanolic extract of *K. galanga* rhizome (EKGR) at 0.5%, 0.75% and 1.0% *w*/*w*, ethyl oleate, a mixed surfactant (Tween 80 and 1,2-hexanediol at 4:1), and water at weight ratios of 0.5:29.5:65:5, 0.75:29.25:65:5, and 1:29:65:5. (**B**) Corresponding SPF values (mean ± SD, $n = 5$). * $p < 0.05$; one-way ANOVA followed by Tukey's HSD test.

3.9. Stability Results of the Ethanolic Extract of K. galanga Rhizome (EKGR)-Loaded Microemulsions

Ethyl *p*-methoxycinnamate (EPMC), the major active compound in EKGR, was used as a chemical marker to assess the stability of ME A–C containing varying oil-phase proportions. After 1 month of storage under various conditions (−20 °C, 4 ± 2 °C, 25 ± 2 °C, and 40 ± 2 °C/75% RH), the EPMC content remained stable (Figure 13A). Notably, a slight increase in EPMC concentration was observed after 1 month, which may be associated with potential evaporation of the volatile components in EKGR, although this was not directly measured in the present study. Therefore, this interpretation should be considered with caution.

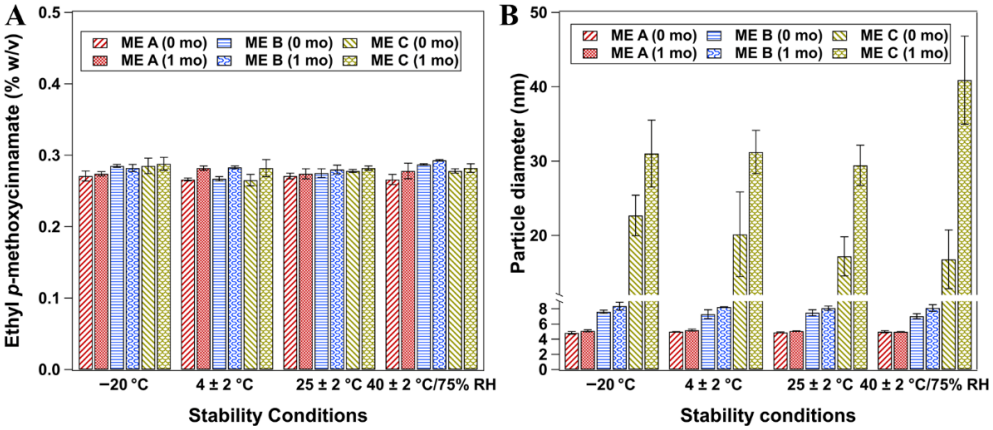


Figure 13. Stability of ME A–C containing 0.5% *w*/*w* of the ethanolic extract of *K. galanga* rhizome (EKGR) after 1 month storage at −20 °C, 4 ± 2 °C, 25 ± 2 °C, and 40 ± 2 °C/75% RH. (**A**) Percentage of assay of ethyl *p*-methoxycinnamate (EPMC) and (**B**) particle size were measured 24 h after preparation and after 1 month of storage ($n = 3$).

Physical stability, assessed via particle size measurements, showed that ME A and ME B maintained their droplet sizes across all storage conditions, indicating good structural stability (Figure 13B). However, the particle size of ME C (30% oil phase) increased noticeably after 1 month at 40 ± 2 °C/75% RH, suggesting potential physical instability. This change may result from enhanced droplet mobility and increased collision frequency at elevated temperatures, promoting coalescence or Ostwald ripening in the high-oil formulation. Despite this, no visible turbidity, cloudiness, or phase separation was observed in any of the formulations.

Overall, these results indicate that EKGR-loaded microemulsions are chemically stable and generally physically stable, with minor susceptibility to particle-size growth in high-oil formulations under accelerated conditions, supporting their potential for cosmetic applications.

4. Discussion

Ultraviolet B (UVB) irradiation is an extrinsic factor driving skin photoaging through the induction of oxidative stress, inflammation, DNA damage, fibroblast senescence and extracellular matrix (ECM) degradation [3,6,9,11,14,16]. In the present study, the ethanolic extract of *K. galanga* rhizome (EKGR) containing ethyl *p*-methoxycinnamate (EPMC) as a major bioactive compound was assessed against UVB-induced cellular senescence and photoaging in human dermal fibroblasts. The key findings include significant attenuation of UVB-induced cellular senescence, increased pro-collagen type I production, and reduced MMP-1 secretion. Additionally, the incorporation of EKGR into a microemulsion system resulted in a concentration-dependent enhancement of SPF, highlighting its dual functionality as both a biological and formulation-active ingredient.

Regarding the inhibition of UVB-induced cellular senescence, SA-β-Gal activity is a widely accepted biomarker of cellular senescence and reflects irreversible growth arrest accompanied by functional deterioration of fibroblasts. UVB irradiation markedly increased SA-β-Gal-positive fibroblasts in this study in line with other previous studies [14,16,39]. Pretreatment with a concentration of 50 µg/mL EKGR significantly reduced SA-β-Gal expression, indicating its ability to attenuate UVB-triggered senescence pathways. Mechanistically, UVB-induced senescence is largely mediated by excessive ROS production, DNA damage accumulation and inflammatory secretion, resulting in the activation of stress-responsive signaling cascades, including p53/p21, p16INK4a/RB and NF-κB/MAPK, mTOR and TGF-β pathways [39–42]. *K. galanga* is rich in bioactive compounds such as EPMC and flavonoids, which have been reported to possess UV absorber [17,25,43], antioxidant [19,25] and anti-inflammatory properties [17,20,21]. In this study, we investigated the UV absorption profile of formulations containing EKGR in the UVB wavelength range. The UV-absorbing capacity of EKGR was concentrated between 280 and 315 nm. UV absorption increased alongside EKGR concentration. UV exposure, especially UVB, affects DNA photoproducts such as cyclobutane pyrimidine dimer (CPD) production. Cell cycle arrest and cellular senescence are responses to the accumulation of DNA damage in cells, and these cellular dysfunctions are considered dominant causative factors of aging [44]. Thus, EKGR could protect cells from DNA damage, instead of UV being absorbed by DNA directly and cell surface receptor activation, induced by UVB directly through its UV-absorbing capacity, being decreased. From a structural perspective, the presence of a conjugated double bond system within the cinnamate skeleton of EPMC and other cinnamate derivatives functions as an internal sun filter at the cellular level [45]. As a consequence, DNA damage and senescence-associated signaling cascades, including the p53/p21 and p16INK4a/Rb pathways, may be suppressed by EPMC-enriched EKGR. Thereby, it may prevent irreversible cell cycle arrest and the onset of cellular senescence. This mechanistic interpretation is con-

sistent with previous findings showing that suppression of p53 acetylation and oxidative stress can effectively inhibit UVB-induced fibroblast senescence [40,41]. Other previous studies have similarly confirmed that sun protection properties can definitely help reduce the harmful effects of UV rays on DNA and protein structural deformation, leading to a reduction in the skin photoaging-related underlying signaling pathway response [44,45].

Increased oxidative stress, induced by UVB, also attacks the DNA, lipids and proteins of skin cells, resulting in the activation of many signaling cascades including p53/p21, p16INK4a/RB, and AP-1/NF-κB transcription factors and the MAPK pathway; this is a significant inducer of accelerated photoaging in skin [39–42]. Exogenous antioxidants counteract reactive oxygen species (ROS) via hydrogen atom transfer, single-electron transfer processes, and the sequestration of catalytic metal ions [19,46]. Regarding the antioxidant property of *Kaempferia galanga* Linn. rhizome, the extract may act by scavenging free radicals and reducing ferric compounds [19]. Additionally, an intracellular antioxidant has been studied and it was reported that pretreatment with EPMC inhibited ROS generation by over 50% in J774.1 macrophages stimulated with H_2O_2 [47]. These activities promote the restoration of the intracellular redox balance between radicals and anti-radicals and suppress senescence-associated signaling, effectively reducing fibroblast senescence. In our current investigation, we found that EKGR could mitigate the proportion of SA-β-Gal-positive fibroblasts induced by UVB significantly. Similar anti-senescence effects have been reported for methanolic extracts enriched with flavonoids derived from related Zingiberaceae species under oxidative stress conditions, supporting the plausibility of this mechanism: quenching intracellular ROS, suppression of metalloproteinase 1 (MMP-1) secretion and extracellular matrix degradation [48,49]. Senescent fibroblasts are known to adopt a senescence-associated secretory phenotype (SASP), characterized by increased secretion of pro-inflammatory cytokines including TNF-α and matrix-degrading enzymes including MMP-1, which selectively cleaves and degrades type I collagen, a principal structural component of the extracellular matrix [42,50]. This study revealed that pretreatment with EKGR prior to UVB irradiation significantly decreased MMP-1 levels in fibroblast culture supernatants, as measured by ELISA. The reduction in MMP-1 may be attributed to direct inhibition of the activation of UVB-activated cell surface receptors, such as the tumor necrosis factor (TNF) receptor, which subsequently activates the downstream MAPK family—specifically p38 MAPK and JNK pathways—leading to enhanced AP-1 and NF-κB transcriptional activity and regulating inflammatory cytokines (including TNF-α and MMP-1). Indirect effects are interfered by excessive ROS production [48,51]. An in vitro and in vivo study conducted by Umar, M.I, et al. reported that EPMC isolated from *K. galanga* extract could inhibit TNF-α production [52]. Therefore, antioxidant and anti-inflammatory phytochemicals in *K. galanga* extract could inhibit these upstream signaling events, thereby reducing TNF-α and MMP-1 gene expression. Moreover, by limiting fibroblast senescence and SASP development, *K. galanga* extract may further decrease the pro-degradative microenvironment responsible for collagen breakdown [19,53], as shown in related family plants, but there have been no studies on this plant yet. Preservation of collagen production and collagen loss are defining features of photoaged skin and results from both increased degradation and impaired biosynthesis. According to the results obtained, UVB exposure significantly reduced collagen production in fibroblasts, whereas pretreatment with EKGR restored collagen levels. The observed enhancement of collagen production is likely a consequence of the dual actions of *K. galanga* extract: suppression of MMP-1-mediated collagen degradation and preservation of non-senescent fibroblast capacity. In addition, UVB-induced ROS and inflammatory signaling are known to inhibit transforming growth factor-β (TGF-β) signaling, a central regulator of collagen synthesis [42,54,55]. By attenuating oxidative stress and inflammatory cytokines, EKGR may help

maintain TGF-β-dependent transcriptional activity and collagen biosynthesis in fibroblasts (study not yet conducted). It has been documented that an ethanolic extract of *K. galanga* accelerates the healing of chemically induced oral mucosal ulcers in Wistar rats through its anti-inflammatory properties [24]. Antioxidant and anti-inflammatory activities are essential conditions for extracellular matrix (ECM) formation and remodeling during the wound healing process and may be associated with TGF-β signaling, which stimulates fibroblasts to produce collagen for tissue repair [56–58].

The findings indicate that *Kaempferia galanga* extract may exert photoprotective effects through an integrated mechanism involving 1. a reduction in UVB-induced DNA damage and receptor activation directly through UVB absorbance; 2. balanced oxidative stress, thereby limiting molecular damage induced by ROS; 3. inhibition of cellular senescence, as evidenced by decreased SA-β-Gal expression; and 4. suppression of MMP-1 secretion, reducing ECM degradation and resulting in collagen restoration. It should be noted that these mechanisms are proposed based on the present findings in conjunction with the previously reported literature, and some were not directly investigated in this study.

EKGR contains UVB-protective molecules that are predominantly lipophilic and chemically unstable in aqueous environments. Incorporating EKGR into microemulsions improves its water solubility and provides a protective environment that enhances stability. To identify suitable microemulsion regions for EKGR loading, two pseudo-ternary phase diagrams consisting of EO, mixed surfactant (T80 and HD at 4:1 or 3:1), and water were constructed. The system with a T80-to-HD ratio of 4:1 was selected because it exhibited a slightly larger single-phase region, which likely arose from a more favorable packing parameter and hydrophilic–lipophilic balance (HLB), therefore facilitating thermodynamically stable droplet formation [28,59]. The higher proportion of T80 increases surfactant coverage at the oil–water interface, reducing interfacial tension, while HD, acting as a medium-chain co-surfactant [60], intercalates between T80 headgroups to enhance interfacial fluidity, further decreasing interfacial tension.

From this phase diagram, three formulations containing 10%, 20%, and 30% oil were selected for characterization. Droplet size increased with increasing oil content, accompanied by a reduction in the presence of larger dispersed domains. In the 10% and 20% oil systems, a secondary large-size population was detected by intensity-weighted DLS (indicated by an asterisk in Table 1); however, number- and volume-weighted distributions revealed only the smaller droplets. This suggests that the large domains correspond to loosely associated aggregates or bridged droplets rather than a distinct, stable dispersed phase. At 30% oil content, droplets were larger but more uniform, with no detectable large aggregates. The higher oil concentration may enhance adsorption of surfactants at droplet surfaces, reducing the number of free surfactants available to form extensive aggregates or bridging structures.

A clear relationship between oil content and viscosity was observed. Viscosity decreased with increasing oil-phase content, likely due to reduced droplet–droplet interactions and the absence of larger surfactant aggregates in more oil-rich systems—consistent with the disappearance of the secondary size population in ME C. Conversely, lower oil formulations exhibited higher viscosities, attributable to increased droplet crowding and transient network formation. Together, the droplet-size and viscosity data indicate subtle yet coherent shifts in microstructural organization as composition varies.

Among the three formulations, ME C was selected for EKGR loading due to its highest oil content (30%), providing greater solubilizing capacity for the lipophilic extract. Dissolving EKGR in ethyl oleate prior to microemulsion formation ensured uniform incorporation and consistent absorption performance. Overall, EKGR-loaded ME C demonstrated good

chemical stability and generally robust physical stability, supporting its suitability as a carrier system for UVB-protective botanical extracts.

These coordinated effects position *K. galanga* extract as a promising natural agent for preventing or ameliorating UVB-induced skin photoaging. There are limitations and future directions despite the robust cellular findings: further studies are needed to delineate the precise molecular pathways involved. Clinical investigations will be essential to validate the translational relevance of *K. galanga* extract for cosmetic or dermatological applications.

5. Conclusions

This study demonstrates that EKGR exerts photoprotective effects at the cellular level via an integrated pathway involving UV absorbance and SA-β-Gal reduction as well as MMP-1 suppression and collagen content preservation in human fibroblasts induced by UVB. Such properties highlight its potential as a natural bioactive ingredient for anti-photoaging skincare to prevent UVB-induced skin damage and maintain skin health. Although EPMC, the major active constituent, exhibits limited hydrophilicity, which may restrict its direct cosmetic application, formulation strategies can overcome this limitation. In this study, EKGR was incorporated into the oil phase of an oil-in-water microemulsion composed of ethyl oleate, mixed surfactants (Tween 80 and 1,2-hexanediol, 4:1), and water to enhance its solubility and formulation stability. The EKGR-loaded microemulsion exhibited UV absorbance, indicating its potential as an SPF-boosting component in cosmetic formulations, and demonstrated good stability throughout the study period. Future research should clarify the molecular mechanisms involved in DNA damage-response genes and senescence-associated protein and mitogen-activated protein kinase pathways in UVB-induced human fibroblasts in more depth. In addition, clinical trials are warranted to evaluate the safety and photoprotective efficacy of EKGR-loaded microemulsions on subjects, specifically assessing their ability to reduce aging signs.

Supplementary Materials: The following supporting information can be downloaded at: https://www.mdpi.com/article/10.3390/cosmetics13020099/s1, Table S1: The composition of microemulsion formulations. Table S2: SPF Calculation for F1. Table S3: SPF Calculation for F0.75. Table S4: SPF Calculation for F0.5.

Author Contributions: K.L. performed the experiment using a cell-based assay, prepared the extracts, analyzed all data, interpreted the data, drafted the original manuscript and revised the final version. J.P. prepared and analyzed the microemulsions, drafted the manuscript, and revised the final version. P.K. performed the experiment using a cell-based assay, prepared the extract and performed the HPLC-UV experiment. N.N. performed the HPLC-UV experiment. M.P. drafted the manuscript. S.Y. revised the manuscript. B.V. designed the experiments; contributed reagents, materials, analysis tools, and data; and revised the manuscript. All authors have read and agreed to the published version of the manuscript.

Funding: This work was financially supported by the Research Grant of Faculty of Pharmaceutical Sciences, Burapha University (Grant no. RX 6/2567).

Institutional Review Board Statement: Not applicable.

Informed Consent Statement: Not applicable.

Data Availability Statement: The authors confirm that the data supporting the findings of this study are available within the article.

Acknowledgments: The authors express their gratitude to the Faculty of Pharmaceutical Sciences at Burapha University for facility support. This work was financially supported by the Research Grant of Faculty of Pharmaceutical Sciences, Burapha University (Grant no. RX 6/2567).

Conflicts of Interest: All authors have no conflicts of interest, and they agree to submit the manuscript to *Cosmetics* as an original research article. This manuscript has not been published elsewhere and is not currently under consideration by another journal.

References

1. Fisher, G.J.; Kang, S.; Varani, J.; Bata-Csorgo, Z.; Wan, Y.; Datta, S.; Voorhees, J.J. Mechanisms of photoaging and chronological skin aging. *Arch. Dermatol.* **2002**, *138*, 1462–1470. [CrossRef]
2. D'Orazio, J.; Jarrett, S.; Amaro-Ortiz, A.; Scott, T. UV radiation and the skin. *Int. J. Mol. Sci.* **2013**, *14*, 12222–12248. [CrossRef]
3. Tiraravesit, N.; Yakaew, S.; Rukchay, R.; Luangbudnark, W.; Viennet, C.; Humbert, P.; Viyoch, J. *Artocarpus altilis* heartwood extract protects skin against UVB in vitro and in vivo. *J. Ethnopharmacol.* **2015**, *175*, 153–162. [CrossRef]
4. Salminen, A.; Kaarniranta, K.; Kauppinen, A. Photoaging: UV radiation-induced inflammation and immunosuppression accelerate the aging process in the skin. *Inflamm. Res.* **2022**, *71*, 817–831. [CrossRef]
5. Ittycheri, A.; Lipsky, W.Z.; Hookway, T.A.; German, G.K. Ultraviolet light induces mechanical and structural changes in full thickness human skin. *J. Mech. Behav. Biomed. Mater.* **2023**, *143*, 105880. [CrossRef]
6. Ansary, T.M.; Hossain, M.R.; Kamiya, K.; Komine, M.; Ohtsuki, M. Inflammatory molecules associated with ultraviolet radiation-mediated skin aging. *Int. J. Mol. Sci.* **2021**, *22*, 3974. [CrossRef] [PubMed]
7. Sullivan, M.; Gonzalez Obezo, C.; Lipsky, Z.; Panchal, A.; Jensen, J. Frontiers in topical photoprotection. *Cosmetics* **2025**, *12*, 96. [CrossRef]
8. Cios, A.; Ciepielak, M.; Szymański, Ł.; Lewicka, A.; Cierniak, S.; Stankiewicz, W.; Mendrycka, M.; Lewicki, S. Effect of different wavelengths of laser irradiation on the skin cells. *Int. J. Mol. Sci.* **2021**, *22*, 2437. [CrossRef]
9. Indirapriyadarshini, R.; Radhiga, T.; Kanimozhi, G.; Prasad, N.R. Preventive effect of andrographolide against ultraviolet-B radiation-induced oxidative stress and apoptotic signaling in human dermal fibroblasts. *Cell Biochem. Funct.* **2023**, *41*, 1370–1382. [CrossRef]
10. Zhang, Z.; Tan, R.; Xiong, Z.; Feng, Y.; Chen, L. Dysregulation of autophagy during photoaging reduce oxidative stress and inflammatory damage caused by UV. *Front. Pharmacol.* **2025**, *12*, 1562845. [CrossRef]
11. Lee, J.J.; Ng, S.C.; Ni, Y.T.; Liu, J.S.; Chen, C.J.; Padma, V.V.; Huang, C.Y.; Kuo, W.W. Protective effects of galangin against H_2O_2/UVB-induced dermal fibroblast collagen degradation via hsa-microRNA-4535-mediated TGFβ/Smad signaling. *Aging* **2021**, *13*, 25342–25364. [CrossRef] [PubMed]
12. Evanti, A.; Wargasetia, T.L.; Gunadi, J.W. Role of *Nigella sativa* L. seed (black cumin) in preventing photoaging (Review). *Biomed. Rep.* **2025**, *23*, 131. [CrossRef]
13. Luangpraditkun, K.; Pimjuk, P.; Phimnuan, P.; Wisanwattana, W.; Wisespongpand, C.; Waranuch, N.; Viyoch, J. Anti-aging properties of *Cannabis sativa* leaf extract against UVA irradiation. *Cosmetics* **2024**, *11*, 45. [CrossRef]
14. Wen, S.Y.; Ng, S.C.; Chiu, Y.T.; Tai, P.Y.; Chen, T.J.; Chen, C.J.; Huang, C.Y.; Kuo, W.W. Enhanced SIRT1 activity by galangin mitigates UVB-induced senescence in dermal fibroblasts via p53 acetylation regulation and activation. *J. Agric. Food Chem.* **2024**, *72*, 23286–23294. [CrossRef]
15. Yuxin, Y.; Hongfu, X.; Xiao, X.; Ben, W.; Rui, D.; Yingzi, L.; Zibo, L.; Jun, W.; Lunquan, S.; Zhili, D.; et al. Ultraviolet A irradiation induces senescence in human dermal fibroblasts by down-regulating DNMT1 via ZEB1. *Aging* **2017**, *10*, 212–228. [CrossRef]
16. Cavinato, M.; Koziel, R.; Romani, N.; Weinmüllner, R.; Jenewein, B.; Hermann, M.; Dubrac, S.; Ratzinger, G.; Grillari, J.; Schmuth, M.; et al. UVB-induced senescence of human dermal fibroblasts involves impairment of proteasome and enhanced autophagic activity. *J. Gerontol. Ser. A Biomed. Sci. Med. Sci.* **2017**, *72*, 632–639. [CrossRef]
17. Chittasupho, C.; Ditsri, S.; Singh, S.; Kanlayavattanakul, M.; Duangnin, N.; Ruksiriwanich, W.; Athikomkulchai, S. Ultraviolet radiation protective and anti-inflammatory effects of *Kaempferia galanga* L. rhizome oil and microemulsion: Formulation, characterization, and hydrogel preparation. *Gels* **2022**, *8*, 639. [CrossRef]
18. Mustafa, R.A.; Hamid, A.A.; Mohamed, S.; Bakar, F.A. Total phenolic compounds, flavonoids, and radical scavenging activity of 21 selected tropical plants. *J. Food Sci.* **2010**, *75*, 28–35. [CrossRef]
19. Wichayapreechar, P.; Charoenjittichai, R.; Prasansuklab, A.; Vinardell, M.P.; Rungseevijitprapa, W. Exploring the in vitro antioxidant, anti-aging, and cytotoxic properties of *Kaempferia galanga* Linn. rhizome extracts for cosmeceutical formulations. *Cosmetics* **2024**, *11*, 97. [CrossRef]
20. Jagadish, P.C.; Latha, K.P.; Mudgal, J.; Nampurath, G.K. Extraction, characterization and evaluation of *Kaempferia galanga* L. (Zingiberaceae) rhizome extracts against acute and chronic inflammation in rats. *J. Ethnopharmacol.* **2016**, *194*, 434–439. [CrossRef]
21. Tewtrakul, S.; Yuenyongsawad, S.; Kummee, S.; Atsawajaruwan, L. Chemical components and biological activities of volatile oil of *Kaempferia galanga* Linn. *Songklanakarin J. Sci. Technol.* **2005**, *27*, 503–507.
22. Suharti, W.S.; Tini, E.W.; Istiqomah, D. Antimicrobial activity of *Kaempferia galanga* against plant pathogen on rice. *Biodiversitas* **2023**, *24*, 1320–1326. [CrossRef]

23. Tara Shanbhag, V.; Chandrakala, S.; Sacchidananda, A.; Kurady, B.L.; Smita, S.; Ganesh, S. Wound healing activity of alcoholic extract of *Kaempferia galanga* in Wistar rat. *Indian J. Physiol. Pharmacol.* **2006**, *50*, 384–390. [PubMed]
24. Suasani Wahyuni, I.; Sufiawati, I.; Nittayananta, W.; Levita, J. Anti-inflammatory activity and wound healing effect of *Kaempferia galanga* L. rhizome on the chemical-induced oral mucosal ulcer in Wistar rats. *J. Inflamm. Res.* **2022**, *15*, 2281–2294. [CrossRef] [PubMed]
25. Panyakaew, J.; Chalom, S.; Sookkheed, S.; Saiaia, A.; Chandeta, N.; Meepowpana, P.; Thavornyutikarna, P.; Mungkornasawakula, P. *Kaempferia* sp. extracts as UV protecting and antioxidant agents in sunscreen. *J. Herbs Spices Med. Plants* **2021**, *27*, 37–56. [CrossRef]
26. Tunsaringkarn, T.; Palanuvej, C.; Rungsiyothin, A.; Issaravanich, S.; Vipunngeun, N.; Chuthaputti, A.; Ruangrungsi, N. Pharmacognostic specification of *Kaempferia galanga* rhizome in Thailand. *J. Health Res.* **2007**, *21*, 207–214.
27. Shaath, N.A. The chemistry of sunscreens. In *Encyclopedia of Aesthetic Rejuvenation Through Volume Enhancement*; Sadick, N.S., Ed.; CRC Press: Boca Raton, FL, USA, 2012; pp. 157–164.
28. Nakajima, H. *IFSCC Monograph No. 7: Microemulsions in Cosmetics*; Micelle Press: Weymouth, UK, 2001.
29. Ingvar, D.; Björn, L. The definition of microemulsion. *Colloids Surf.* **1981**, *3*, 391–392. [CrossRef]
30. Shinoda, K.; Lindman, B. Organized surfactant systems: Microemulsions. *Langmuir* **1987**, *3*, 135–149. [CrossRef]
31. Scomoroscenco, C.; Teodorescu, M.; Burlacu, S.G.; Gîfu, I.C.; Mihaescu, C.I.; Petcu, C.; Raducan, A.; Oancea, P.; Cinteza, L.O. Synergistic antioxidant activity and enhanced stability of curcumin encapsulated in vegetal oil-based microemulsion and gel microemulsions. *Antioxidants* **2022**, *11*, 854. [CrossRef]
32. Lv, X.; Liu, T.; Ma, H.; Tian, Y.; Li, L.; Li, Z.; Gao, M.; Zhang, J.; Tang, Z. Preparation of essential oil-based microemulsions for improving the solubility, pH stability, photostability, and skin permeation of quercetin. *AAPS PharmSciTech* **2017**, *18*, 3097–3104. [CrossRef]
33. Lv, X.; Cong, Z.; Liu, Z.; Ma, X.; Xu, M.; Tian, Y.; Zhang, X.; Xu, B.; Zhang, J.; Tang, Z. Improvement of the solubility, photostability, antioxidant activity and UVB photoprotection of trans-resveratrol by essential oil based microemulsions for topical application. *J. Drug Deliv. Sci. Technol.* **2018**, *48*, 346–354. [CrossRef]
34. Adianingsih, O.R.; Ihsan, B.R.P.; Puspita, O.E.; Maesayani, K.S. Validation of high-performance liquid chromatography (HPLC) method for quantification of ethyl p-methoxycinnamate in *Kaempferia galanga* extract. *Trop. J. Nat. Prod. Res.* **2023**, *7*, 3829–3835. [CrossRef]
35. Dutra, E.A.; Oliveira, D.A.G.C.; Kedor-Hackmann, E.R.M.; Santoro, M.I.R.M. Determination of sun protection factor (SPF) of sunscreens by ultraviolet spectrophotometry. *Rev. Bras. Ciências Farm.* **2004**, *40*, 381–385. [CrossRef]
36. Sayre, R.M.; Agin, P.P.; LeVee, G.J.; Marlowe, E. A comparison of in vivo and in vitro testing of sunscreening formulas. *Photochem. Photobiol.* **1979**, *29*, 559–566. [CrossRef]
37. Paul, B.; Moulik, S. The viscosity behaviours of microemulsions: An overview. *Proc. Indian Natl. Sci. Acad.* **2000**, *66*, 499–519.
38. Salager, J.L.; Marquez, R.; Rondón, M.; Bullón, J.; Graciaa, A. Review on some confusion produced by the bicontinuous microemulsion terminology and its domains microcurvature: A simple spatiotemporal model at optimum formulation of surfactant–oil–water systems. *ACS Omega* **2023**, *8*, 9040–9057. [CrossRef]
39. Wang, J.; Yuan, M.; Li, Q.; Shen, C.; Zhang, X.; Zhu, C.; Cen, O. Combined protection against UVB-induced photoaging by oleuropein, hydroxytyrosol, and verbascoside through modulation of inflammation, oxidative stress, and collagen homeostasis. *Sci. Rep.* **2025**, *15*, 41008. [CrossRef]
40. Safwan-Zaiter, H.; Wagner, N.; Wagner, K.D. P16INK4A-more than a senescence marker. *Life* **2022**, *12*, 1332. [CrossRef]
41. Chung, K.W.; Choi, Y.J.; Park, M.H.; Jang, E.J.; Kim, D.H.; Park, B.H.; Yu, B.P.; Chung, H.Y. Molecular insights into SIRT1 protection against UVB-induced skin fibroblast senescence by suppression of oxidative stress and p53 acetylation. *J. Gerontol. Ser. A Biomed. Sci. Med. Sci.* **2015**, *70*, 959–968. [CrossRef]
42. Nan, L.; Guo, P.; Hui, W.; Xia, F.; Yi, C. Recent advances in dermal fibroblast senescence and skin aging: Unraveling mechanisms and pioneering therapeutic strategies. *Front. Pharmacol.* **2025**, *16*, 1592596. [CrossRef] [PubMed]
43. Wang, S.Y.; Zhao, H.; Xu, H.T.; Han, X.D.; Wu, Y.S.; Xu, F.F.; Yang, X.B.; Göransson, U.; Liu, B. *Kaempferia galanga* L.: Progresses in phytochemistry, pharmacology, toxicology and ethnomedicinal uses. *Front. Pharmacol.* **2021**, *12*, 675350. [CrossRef] [PubMed]
44. Lee, J.J.; Kim, K.B.; Heo, J.; Cho, D.H.; Kim, H.S.; Han, S.H.; Ahn, K.J.; An, I.S.; An, S.; Bae, S. Protective effect of *Arthrospira platensis* extracts against ultraviolet B-induced cellular senescence through inhibition of DNA damage and matrix metalloproteinase-1expression in human dermal fibroblasts. *J. Photochem. Photobiol. B* **2017**, *173*, 196–203. [CrossRef] [PubMed]
45. Gupta, A.; Singh, A.P.; Singh, V.K.; Singh, P.R.; Jaiswal, J.; Kumari, N.; Upadhye, V.; Singh, S.C.; Sinha, R.P. Natural sun-screening compounds and DNA-repair enzymes: Photoprotection and photoaging. *Catalysts* **2023**, *13*, 745. [CrossRef]
46. Kotha, R.R.; Tareq, F.S.; Yildiz, E.; Luthria, D.L. Oxidative stress and antioxidants—A critical review on in vitro antioxidant assays. *Antioxidants* **2022**, *11*, 2388. [CrossRef]

47. Srivastava, N.; Ranjana; Singh, S.; Gupta, A.C.; Shanker, K.; Bawankule, D.U.; Luqman, S. Aromatic ginger (*Kaempferia galanga* L.) extracts with ameliorative and protective potential as a functional food, beyond its flavor and nutritional benefits. *Toxicol. Rep.* **2019**, *6*, 521–528. [CrossRef]
48. Ahn, S.Y.; Jeong, S.Y.; Lee, B.S.; Joh, Y.S.; Hamishehkar, H.; Lee, S.; Kim, K.H. Anti-skin aging potential of methoxyflavones from *Kaempferia parviflora* against TNF-α-induced oxidative stress and photoaging in normal human dermal fibroblasts. *Foods* **2025**, *14*, 4012. [CrossRef]
49. Klinngam, W.; Rungkamoltip, P.; Thongin, S.; Joothamongkhon, J.; Khumkhrong, P.; Khongkow, M.; Namdee, K.; Tepaamorndech, S.; Chaikul, P.; Kanlayavattanakul, M. Polymethoxyflavones from *Kaempferia parviflora* ameliorate skin aging in primary human dermal fibroblasts and ex vivo human skin. *Biomed. Pharmacother.* **2022**, *145*, 112461. [CrossRef]
50. Ghosh, K.; Capell, B.C. The senescence-associated secretory phenotype: Critical effector in skin cancer and aging. *J. Investig. Dermatol.* **2016**, *136*, 2133–2139. [CrossRef]
51. Lee, J.S.; Min, J.W.; Gye, S.B.; Kim, Y.W.; Kang, H.C.; Choi, Y.S.; Seo, W.S.; Lee, B.Y. Suppression of UVB-induced MMP-1 expression in human skin fibroblasts using lysate of *Lactobacillus iners* derived from Korean women's skin in their twenties. *Curr. Issues Mol. Biol.* **2024**, *46*, 513–526. [CrossRef]
52. Umar, M.I.; Asmawi, M.Z.; Sadikun, A.; Majid, A.M.; Al-Suede, F.S.; Hassan, L.E.; Altaf, R.; Ahamed, M.B. Ethyl-p-methoxycinnamate isolated from *Kaempferia galanga* inhibits inflammation by suppressing interleukin-1, tumor necrosis factor-α, and angiogenesis by blocking endothelial functions. *Clinics* **2014**, *69*, 134–144. [CrossRef]
53. Park, J.E.; Pyun, H.B.; Woo, S.W.; Jeong, J.H.; Hwang, J.K. The protective effect of *Kaempferia parviflora* extract on UVB-induced skin photoaging in hairless mice. *Photodermatol. Photoimmunol. Photomed.* **2014**, *30*, 237–245. [CrossRef] [PubMed]
54. Fisher, G.J.; Quan, T.; Purohit, T.; Shao, Y.; Hei, T.K.; Xu, H.; Wang, Z.Q.; Varani, J.; Kang, S.; Voorhees, J.J. Solar ultraviolet irradiation reduces collagen in photoaged human skin by blocking transforming growth factor-β type II receptor/Smad signaling. *Int. J. Mol. Sci.* **2002**, *3*, 69–81.
55. Pittayapruek, P.; Meephansan, J.; Prapapan, O.; Komine, M.; Ohtsuki, M. Role of ROS/MAPK/AP-1 signaling in mediating photoaging and the downregulation of TGF-β-dependent collagen synthesis in human skin fibroblasts. *Antioxidants* **2016**, *5*, 28. [CrossRef]
56. Wolosik, K.; Chalecka, M.; Gasiewska, G.; Palka, J.; Surazynski, A. Squalane as a promising agent protecting UV-induced inhibition of collagen biosynthesis and wound healing in human dermal fibroblast. *Molecules* **2025**, *30*, 1964. [CrossRef]
57. Viaña-Mendieta, P.; Sánchez, M.L.; Benavides, J. Rational selection of bioactive principles for wound healing applications: Growth factors and antioxidants. *Int. Wound J.* **2022**, *19*, 100–113. [CrossRef]
58. Wang, G.; Yang, F.; Zhou, W.; Xiao, N.; Luo, M.; Tang, Z. The initiation of oxidative stress and therapeutic strategies in wound healing. *Biomed. Pharmacother.* **2023**, *162*, 114004. [CrossRef] [PubMed]
59. Tartaro, G.; Mateos, H.; Schirone, D.; Angelico, R.; Palazzo, G. Microemulsion microstructure(s): A tutorial review. *Nanomaterials* **2020**, *10*, 1657. [CrossRef]
60. Raman, I.A.; Lye, O.T.; Ahmad, S.; Suhaimi, H. 1,2-Hexanediol as an alternative cosurfactant for preparing palm-based microemulsions for practical applications. *J. Dispers. Sci. Technol.* **2008**, *29*, 1003–1009. [CrossRef]

Disclaimer/Publisher's Note: The statements, opinions and data contained in all publications are solely those of the individual author(s) and contributor(s) and not of MDPI and/or the editor(s). MDPI and/or the editor(s) disclaim responsibility for any injury to people or property resulting from any ideas, methods, instructions or products referred to in the content.